STONELEY WAVE PROPAGATION IN HETEROGENEOUS PERMEABLE POROUS FORMATIONS

by

Xiaomin Zhao, M.N. Toksöz, and C.H. Cheng

Earth Resources Laboratory
Department of Earth, Atmospheric, and Planetary Sciences
Massachusetts Institute of Technology
Cambridge, MA 02139

ABSTRACT

The propagation of borehole Stoneley waves is strongly correlated with permeability of the formation. Previous studies primarily focused on the situation where the permeability is homogeneously distributed in the formation. In many in-situ situations, however, the permeability distribution of the formation is heterogeneous, due to effects such as a damaged zone around the borehole, random variation of the formation permeability, and layering, etc. This study investigates the effects of formation permeability heterogeneity on Stoneley wave propagation. Using the theory of dynamic permeability and a finite difference technique in cylindrical coordinates, dynamic pore fluid flow in an arbitrarily heterogeneous porous medium surrounding the borehole is modeled. The effects of the flow on the borehole Stoneley waves are calculated. The calculations were performed on various types of permeability heterogeneities. For a formation having random permeability variation with various heterogeneity scale lengths (smaller than the scale of the borehole), the Stoneley wave attenuation and dispersion are only slightly higher than those calculated with a constant permeability (mean value of the random distributions). For a formation with permeability linearly increasing or decreasing away from the borehole, the Stoneley wave behaviors are also similar to those calculated with a constant permeability. Significant effects are found for a damaged zone case where the zone has much higher permeability than the virgin formation. The attenuation exhibits a peak and the Stoneley wave velocity is significantly decreased in the frequency range from 0 to 3 kHz. These features, if measured from the data, can be used as a diagnostic of the borehole condition.

INTRODUCTION

Stoneley waves in porous boreholes are sensitive to formation permeability. Intensive research has been carried out to study the effects of permeability on Stoneley waves (Rosenbaum, 1974; Schmitt et al., 1988; Cheng et al., 1987;, Chang et al., 1988; Tang et al., 1991a). In most of the previous studies, permeability distribution in the formation was assumed homogeneous. In many situations, however, permeability changes in the formation. For example, the damaged borehole wall due to drilling results in higher permeability of the immediate surrounding formation than the virgin formation. Schmitt et al. (1988), have studied the effects of a damaged zone, where the permeability of the damaged zone is moderately different from that of the virgin formation. Mud filtration into the formation may also change the formation flow property along the radial direction. The random variation of the porous formation is also an example of heterogeneous permeability. Because of the heterogeneous formation flow properties, the propagation of borehole Stoneley waves will be modified compared to the homogeneous case. Therefore, the study of Stoneley wave propagation in the presence of heterogeneous formation permeability will help develop methods for characterizing these heterogeneities.

The effective technique to handle medium heterogeneities is the finite difference method. However, the application of this technique with Biot poroelastic theory (Biot, 1956a,b) to model acoustic wave propagation in porous boreholes is still a topic of research. The difficulty lies in the coupling of the pore fluid motion (i.e., the Biot slow wave) with the motion of the elastic solid and the strong dispersive nature of the slow wave. Recent study by Tang et al. (1991b) has shown that the interaction of the borehole Stoneley wave with the porous formation can be decomposed into two parts. One is the interaction with the motion of the formation elastic solid (equivalent elastic formation) and the other is with the pore fluid flow. The advantage of this decomposition is that, given the solution of the elastic problem, one can solve the pore fluid flow problem for the heterogeneous porous formation independent of the elastic problem. The combination of the two situations will give the solution for Stoneley wave propagation in the formation with heterogeneous permeability.

The behavior of dynamic fluid flow in heterogeneous porous media has been modeled by Zhao et al. (1992) for the Cartesian coordinates. Because of the dispersive nature of the flow motion, an iterative finite difference technique was developed to compute the flow field in the frequency domain. For the present borehole geometry, we need to solve the dynamic fluid flow problem for the cylindrical coordinate system. The iterative finite difference technique for the cylindrical system will be developed in this study. With this technique, the borehole Stoneley wave propagation in the presence of various formation permeability heterogeneities will be studied.

THEORY OF STONELEY WAVE PROPAGATION IN PERMEABLE BOREHOLES

For a Stoneley wave propagating in a permeable porous borehole, the interaction of the Stoneley wave with the formation can be decomposed into two parts (Tang et al., 1991b). The first is the interaction with an equivalent elastic formation, and the second is the interaction with the dynamic fluid flow into the formation. Tang and Cheng (1993) have shown that the Stoneley wave can be described by the following one-dimensional wave equation:

$$\frac{d^2P}{dz^2} + \left[\frac{\omega^2}{v_f^2} + \frac{2\rho_f\omega^2}{R}\frac{U_e}{P} + \frac{2i\rho_f\omega\phi}{R}\frac{\overline{V}_f}{P}\right] P = 0 \ , \tag{1}$$

where

P = borehole pressure associated with Stoneley wave
U_e = radial elastic displacement of borehole wall
R = borehole radius
v_f = acoustic speed of borehole fluid
ρ_f = density of borehole fluid
ω = angular frequency
ϕ = formation porosity
$\overline{V}_f$ = average pore fluid flow velocity at borehole wall.

If the radial flow velocity V_f changes with azimuthal direction θ, $\overline{V}_f$ is given by

$$\overline{V}_f = \frac{1}{2\pi}\int_0^{2\pi} V_f(\theta)d\theta \ . \tag{2}$$

Eq. (1) shows that the Stoneley wave has a wavenumber given by

$$k = \sqrt{\frac{\omega^2}{v_f^2} + \frac{2\rho_f\omega^2}{R}\frac{U_e}{P} + \frac{2i\rho_f\omega}{R}\frac{\phi\overline{V}_f}{P}} \ . \tag{3}$$

This equation indicates that the Stoneley wave propagation in a porous borehole is affected by formation elastic displacement U_e and the pore fluid flow $\overline{V}_f$. If the borehole wall is impermeable, i.e., $\overline{V}_f = 0$, then the Stoneley wavenumber becomes

$$k_e = \sqrt{\frac{\omega^2}{v_f^2} + \frac{2\rho_f\omega^2}{R}\frac{U_e}{P}} \quad . \tag{4}$$

This wavenumber is the Stoneley wavenumber for the equivalent elastic formation. The elastic properties of the formation are those of the fluid-saturated rocks (Tang et al., 1991b). The objective of the present study is, given the solution of the elastic problem, compute the formation flow $\overline{V}_f$ due to heterogeneous permeability and study its effects on the Stoneley wave propagation using the following equation

$$k = \sqrt{k_e^2 + \frac{2i\rho_f\omega}{R}\frac{\overline{V}_f\phi}{P}} \quad . \tag{5}$$

That is, if we can compute the flow per unit pressure $\overline{V}_f/P$ into the formation of given permeability distribution, then we can substitute the $\overline{V}_f/P$ value and the given k_e into (5) to obtain the Stoneley wavenumber for the heterogeneous permeability formation. From this wavenumber, the Stoneley wave attenuation (expressed as $1/Q$) and phase velocity are computed using

$$\begin{cases} \frac{1}{Q} &= 2\frac{Im(k)}{Re(k)} \\ v_{st} &= \frac{\omega}{Re(k)} \end{cases} \quad . \tag{6}$$

DYNAMIC FLUID FLOW IN CYLINDRICAL COORDINATES

The dynamic fluid flow in heterogeneous permeability media is described by the following equation (Zhao et al., 1992)

$$\nabla \cdot [\alpha(\omega, \vec{x})\nabla p] + i\omega p = 0 \quad , \tag{7}$$

where p is dynamic pressure associated with pore fluid motion,

$$\alpha(\omega, \vec{x}) = \frac{\kappa(\omega, \vec{x})K_f}{\phi\mu(1+\xi)} \tag{8}$$

is dynamic pore fluid diffusivity, K_f = fluid incompressibility, ϕ = porosity, μ = fluid viscosity, and ξ is a correction for solid matrix compressibility (Norris, 1989). In this

study, we neglect the effect of solid compressibility (i.e., $\xi = 0$). This effect is minor if the fluid is much more compressible than the rock. The fluid diffusivity $\alpha(\omega, \vec{x})$ is a function of both frequency and the spatial position $\vec{x}$. This happens if the dynamic permeability (Johnson et al., 1987)

$$\kappa(\omega, \vec{x}) = \frac{\kappa_0(\vec{x})}{\left(1 - \frac{i}{2}\tau\kappa_0(\vec{x})\rho_0\omega/\mu\phi\right)^{\frac{1}{2}} - i\frac{\tau\kappa_0(\vec{x})\rho_0\omega}{\mu\phi}} \tag{9}$$

is a function of the spatial position when the static permeability $\kappa_0(\vec{x})$ varies with $\vec{x}$. In Eq. (9), τ is tortuosity of the porous medium, ρ_0 the pore fluid density.

For the borehole configuration, the cylindrical coordinates are most convenient to use. In this study, we investigate a two-dimensional (2-D) case where the permeability variation is in the radial (r) and azimuthal (θ) directions, i.e.,

$$\kappa_0(\vec{x}) = \kappa_0(r, \theta) \ . \tag{10}$$

In the cylindrical system, Eq. (7) becomes

$$\frac{\partial}{\partial r}\left(\alpha(r,\theta)\frac{\partial p}{\partial r}\right) + \frac{\alpha(r,\theta)}{r}\frac{\partial p}{\partial r} + \frac{1}{r^2}\frac{\partial}{\partial \theta}\left(\alpha(r,\theta)\frac{\partial p}{\partial \theta}\right) + \alpha(r,\theta)\frac{\partial^2 p}{\partial z^2} + i\omega p = 0 \ . \tag{11}$$

Due to the excitation of a propagating borehole Stoneley wave e^{ikz} (as first order perturbation, e^{ikz} can be replaced by $e^{ik_e z}$, see Tang et al., 1991b), the pore fluid pressure can be written as

$$p(r, \theta, z) = p(r, \theta)e^{ik_e z} \ . \tag{12}$$

By substituting Eq. (12) into Eq. (11), Eq. (11) becomes

$$\frac{\partial}{\partial r}\left(\alpha\frac{\partial p}{\partial r}\right) + \frac{\alpha}{r}\frac{\partial p}{\partial r} + \frac{\alpha}{r^2}\frac{\partial}{\partial \theta}\left(\alpha\frac{\partial p}{\partial \theta}\right) + (i\omega - \alpha k_e^2)p = 0 \ . \tag{13}$$

Eq.(13) is the 2-D partial differential equation of dynamic flow for the heterogeneous permeability distribution $\kappa_0(r, \theta)$. Because Eq. (13) is a Helmholtz type equation, an iterative method (Zhao and Toksöz, 1992) based on the Alternating Direction Implicit (ADI) finite difference algorithm (Ferziger, 1981) is used to solve the equation. The boundary conditions for the problem are

$$p(r,\theta)|_{r=R} = P \quad \text{(pressure continuity)} \tag{14}$$
$$p(r,\theta)|_{r=\infty} = 0 \quad \text{(radiation condition)} \tag{15}$$

The detailed finite difference solution procedure of Eq. (13) is described in the Appendix.

From the finite difference solution, we can compute the pressure distribution $p(r, \theta; \omega)$ over the (r, θ) grid. The fluid flow at the borehole wall is computed using the modified Darcy's law (Tang et al., 1991a)

$$\phi \overline{V}_f = -\frac{1}{2\pi} \int_0^{2\pi} \left\{ \frac{\kappa(r,\theta;\omega)}{\mu} \frac{dp(r,\theta)}{dr} |_{r=R} \right\} d\theta \tag{16}$$

where $\frac{dp(r,\theta)}{dr}$ is numerically evaluated from the calculated pressure field at the borehole wall. Because $\overline{V}_f$ is proportional to the borehole pressure P, the ratio $\overline{V}_f/p|_{r=R} = \overline{V}_f/P$ is independent of the magnitude of P. Substituting $\overline{V}_f/P$ into Eq. (5), the Stoneley wavenumber can be calculated. From the wavenumber, the Stoneley wave attenuation and phase velocity can be calculated using Eq. (6).

NUMERICAL SIMULATION RESULTS

In this section, we present the finite difference simulation results for various permeability distributions surrounding the borehole. For all the calculations below, we first calculate the elastic problem using the saturated rock properties: $v_p = 4000$ m/s, $v_s = 2300$ m/s, and $\rho = 2.65$ g/cm^3. The Stoneley wavenumber k_e for the equivalent elastic formation is calculated using the borehole dispersion equation (Cheng and Toksöz, 1981). The borehole fluid density and velocity are $\rho_f = 1$ g/cm^3 and $v_f = 1500$ m/s, respectively. The borehole radius is 0.1 m. For simplicity, we assume that elastic properties for the various heterogeneous permeability distributions are the same, so that the same k_e is used for the following cases. In all the cases below, the pore fluid properties are: $K_f = 2.25$ GPa, $\rho_0 = 1$ g/cm^3, $\mu = 1.14$ cp, porosity $\phi = 0.3$, and tortuosity $\tau = 3$.

Homogeneous Permeability – A Test of the Numerical Algorithm

We first present the simulation result for a homogeneous permeability surrounding the borehole. This example, together with the existing analytical solution, offers a test of the validity and accuracy of the finite difference simulation algorithm.

For homogeneous permeability, the solution to Eq. (13) becomes

$$p(r) = \frac{K_0(r\sqrt{-\frac{i\omega}{\alpha} + k_e^2})}{K_0(R\sqrt{-\frac{i\omega}{\alpha} + k_e^2})} \tag{17}$$

and the Stoneley wavenumber for the permeable formation is (Tang et al., 1991b)

$$k = \sqrt{k_e^2 + \frac{2i\rho_f\omega\phi}{R\mu}\sqrt{-\frac{i\omega}{\alpha} + k_e^2}\frac{K_1(R\sqrt{-i\omega/\alpha + k_e^2})}{K_0(R\sqrt{-i\omega/\alpha + k_e^2})}} \ , \tag{18}$$

where α is given by Eqs. (8) and (9), in which the static permeability κ_0 is a constant. In Eqs. (17) and (18), K_n $(n = 0, 1)$ is the second kind Modified Bessel function. The Stoneley wave velocity and attenuation calculated using Eq. (6) agree with the results calculated with the full Biot theory very well (Tang et al., 1991b), although in this much simplified theory, the coupling between the motion of the solid matrix and the dynamic flow (i.e., the coupling between the fast (compressional and shear) waves and the slow wave) is not fully considered. This tells us that if the dynamic fluid flow in heterogeneous permeability porous media can be accurately modeled using the finite difference technique, then the effects of the heterogeneous permeability on the Stoneley wave propagation can be calculated using the simple formula given in Eq. (5).

Figure 1a shows the comparison between the Stoneley wave phase velocity (a) and attenuation (b) calculated using the analytical solution (Eq. 18) and those using the finite difference method. These results are calculated for the frequency range of $0 \sim 5$ kHz, in which most Stoneley wave measurements are made. The formation permeability is 1 Darcy. For simplicity, the effect due to solid matrix compressibility is neglected (i.e., $\xi = 0$ in Eq. 8) when calculating both the analytical and finite difference results. The results for the two difference approaches are in excellent agreement. This comparison demonstrates the validity and accuracy of the finite difference technique. In the case of a heterogeneous permeability distribution where an analytical solution is difficult to find, we can rely on the finite difference method to calculate the Stoneley wave propagation.

Random Permeability Distributions

In a geological porous medium, the permeability of the medium may fluctuate from place to place. These fluctuations can be modeled by describing the medium as having a random permeability distribution. Zhao et al. (1992) have modeled the dynamic pore fluid flow in such a random medium. It is interesting to investigate how this random variation of formation permeability affects the borehole Stoneley wave propagation and

how the random permeability heterogeneities can best be characterized using Stoneley wave measurements.

The method of generating 2-D random variations in Cartesian coordinates were descibed in Zhao and Toksöz (1991). A 2-D random field is first generated by Gaussian distribution. Then the 2-D field is convolved with a chosen correlation function of given correlation length, yielding a random field with clustered structures. Figure 2 shows an example of the random permeability distribution with a borehole of 0.2 m diameter at the center. The distribution is generated with a Gaussian correlation function having a correlation length of 0.08 m. The standard deviation of the random field is 38% of the mean value (average of the random field). It can be seen that the permeability varies significantly in the formation surrounding the borehole. It is interesting to see how this permeability fluctuation affects the Stoneley wave propagation in the borehole and how the results compare with those calculated with the constant permeability distribution.

For calculating the dynamic pore fluid flow in the cylindrical coordinates, the permeability distribution in Cartesian coordinates is mapped into cylindrical coordinates using

$$\kappa_0(x,y) \overset{x=r\cos\theta, y=r\sin\theta}{\longrightarrow} \kappa_0(r,\theta) \quad . \tag{19}$$

For the distribution $\kappa_0(x,y)$ in the equally-spaced grids (x,y), its mapping into the (r,θ) coordinates is distributed over a (r,θ) grid that is not equally-spaced. But the finite difference grid requires the equally-spaced grid. This problem is solved by interpolating the mapped values of $\kappa_0(r,\theta)$ to the finite difference grids.

Figure 3 shows the finite difference simulation of pore fluid presure amplitude distribution at 100 Hz for the permeability distribution in Figure 2. The correlation length of this distribution is 0.08 m, and the mean permeability is 1 Darcy. For a constant permeability distribution, the pressure contours should be circular in shape. The non-circular shape of the pressure contours in Figure 3 demonstrates the effects of the heterogeneous permeability. The Stoneley wave phase velocity and attenuation for the heterogeneous permeability in Figure 2 are shown in Figure 4. For the fixed correlation length and mean permeability, the calculation is performed for two fluctuation values, one is 20% (dashed line 1), the other is 38% (dashed line 2). The results are plotted versus those calculated with a constant permeability that is equal to the mean value of the random permeability distribution (solid line). To our suprise, both the Stoneley phase velocity and attenuation for the random permeability are only slightly different from those for the constant permeability case. The 20% curves are very close to the constant permeability curve, while the 38% case shows more attenuation and dispersion than the constant permeability case.

These results are not difficult to understand because the Stoneley wave tends to

average out the azimuthal permeability variation (see Eq. 16), such that the random permeability medium behaves like a constant permeability medium. The important implication of this is that, for Stoneley waves measured in formations with randomly fluctuating permeability, the analytical result for the constant permeability medium (Eq. 17) is a very good description, if we regard the constant permeability κ_0 as the mean permeability of the random medium. To account for the increased attenuation and dispersion, we can interpret the medium as a homogeneous medium having a slightly higher permeability than the mean permeability of the actual random medium.

Layered Model

We next discuss an interesting situation in which the permeability distribution has a layered structure and the borehole axis is parallel to the layering. We will encounter this situation in a horizontal well drilled through horizontal bedding layers.

We first study the case where the permeability varies smoothly across the layers. We model this by generating the random permeability distributions using a flat-ellipse-shaped Gaussian correlation function, in which the correlation length in the semi-major direction is much greater than the correlation length along the semi-minor direction. The procedure is described in detail in Zhao and Toksöz (1991). Figure 5 shows the configuration of the borehole in the smoothly varying layered media (a). The correlation length in the elongated direction is 0.23 m, where that in the direction normal to the layering is 0.05 m. The standard deviation of permeability is 38%. The mean permeability is 1 Darcy. The calculated Stoneley wave velocity and attenuation are shown in Figure 6(a) and (b) (solid curves), respectively. The results calculated using the constant permeability (1 Darcy) are also plotted. As for the isotropic random-permeability distribution cases (Figure 4), the results for the layered permeability distribution are not much different from those of the constant permeability.

Next we study the case in which the layers have strong permeability contrast, such as the sand-shale sequences. We generate this model using a random repetition of layers with low and high permeabilities (they are 0.01 and 2 Darcy, respectively). The thickness of the layers obey a Poisson distribution (Kerner, 1992). The average thickness of the layers is 0.1 m. Figure 7 shows the configuration of the borehole in the layered medium with alternating permeabilities. The calculated Stoneley wave velocity and attenuation are shown in Figure 8(a) and (b) (solid curves), respectively. The results for the average permeability (1 Darcy) are also shown (dashed curves). Again, the layered model results are very similar to the constant permeability results.

The simulation for the layered permeability models shows that the Stoneley wave propagation is not sensitive to the anisotropy in the permeability distribution. This can be expected since the Stoneley wave sums the effects of pore fluid flow at the borehole

wall in all azimuthal directions (see Eq. 2). If the high and low permeability regions alternate around the borehole wall, as is the case for the above two examples, then the effects of the heterogeneous permeability formation affects the borehole Stoneley wave in much the same way as does a homogeneous formation having the average permeability of the heterogeneous formation.

Mud Filtration Model

In a mud-filled borehole, the filtration (or invasion) of mud into the porous formation may result in the replacement or mixing of mud with formation saturant fluid, resulting in the change of fluid flow properties in the radial direction. For example, if the viscosity of mud is different from that of the virgin saturant fluid, the fluid mobility (expressed as κ_0/μ) may decrease or increase away from the borehole, assuming that μ equals mud viscosity at the borehole wall and formation saturant fluid viscosity far from borehole. Alternatively, this change of fluid mobility may also be modeled as a change of the permeability, if we fix viscosity μ as a constant and vary permeability. Therefore, we can model the mud filtration effects using the variable permeability model.

We consider two simple cases. One is that the permeability linearly increases from 0.1 Darcy at the borehole wall to a value of 1 Darcy at $R = 1m$ (viscosity decreases in the radial direction). The other case is that the permeability linearly decreases from a value of 1 Darcy at the borehole wall ($R_0 = 0.1m$) to 0.1 Darcy at $R = 1m$ (viscosity increases). Figure 9 shows the modeled Stoneley wave dispersion (a) and attenuation (b) as a function of frequency. For comparison, the results for constant permeabilities 0.1 and 1 Darcy are also plotted. In general, the behaviors of the velocity and attenuation for the linear permeability model are similar to that of the constant permeability case, the dispersion and attenuation all increasing with decreasing frequency. Because the depth of penetration of fluid flow is very small, the attenuation and dispersion of the variable permeability model are very close to those calculated with the constant permeability having a value equal to that of the borehole wall. For the increasing permeability ($0.1 - 1$) model, the results are almost the same as those calculated with the constant permeability of 0.1 Darcy. For the decreasing permeability ($1 - 0.1$) model, the results only slightly differ from the constant permeability (1 Darcy) model at higher frequencies. These results suggest that for permeability decreasing or increasing smoothly from the borehole, the Stoneley wave is mainly sensitive to the permeability of the immediate surrounding borehole.

Damaged Zone Model

During the drilling of a borehole, the drilling process can change the physical properties of the formation close to the borehole wall. For example, due to the drilling damage,

vertical micro fractures and fissures may exist at the borehole wall, resulting in the immediate surrounding formation having much higher permeability than the virgin formation. An example is illustrated in Figure 10. As will be shown below, this high permeability contrast produces significant effects on the Stoneley wave propagation.

The first example considered is a case in which the permeability decreases away from the borehole wall. The damaged zone is modeled as a porous layer of 5 cm thick. The zone and the formation are assumed to have the same porosity and are water saturated. The permeability for the layer and the formation are 1.0 and 0.3 Darcy, respectively. Figure 11 shows the calculated dispersion and attenuation curves, in comparison with the results calculated for the constant permeability of 1.0 and 0.3 Darcy. At low frequencies, the velocity and attenuation are sensitive to the virgin formation permeability. Particularly for the attenuation, the attenuation value tends to approach that calculated for the virgin permeability at very low frequencies. As frequency increases, the results approach those for the damaged zone, becoming representative of the inner layer properties. These results are similar to those obtained by Schmitt et al. (1988) using the full Biot theory. For the case of moderate permeability contrast, the behavior of Stoneley wave propagation is not significantly different from Stoneley wave behavior in a formation of constant permeability, except at very low frequencies.

The next example corresponds to a strong permeability contrast case in which the inner layer permeability is very high (10 Darcy). This high permeability could result from vertical micro fractures surrounding the borehole wall, when the wall is intensely damaged. The zone thickness is assumed to be 0.11 m. The results are calculated with virgin formation permeability equal to 1 and 0.1 Darcy, respectively. Figure 12 shows the dispersion (a) and attenuation (b) curves for the first case (virgin permeability = 1 Darcy). For comparison, the results for the constant permeabilities (1 and 10 Darcy, respectively) are also plotted. Figure 13 shows the results for the second case (virgin permeability = 0.1 Darcy). The results for the two very different virgin permeability cases have similar behavior. At very low frequencies, the Stoneley wave attenuation is very close to those due to the virgin formation. As frequency increases, the attenuation significantly increases, and then decreases to approach the attenuation due to the inner layer, showing a well defined peak in the frequency range between $0 \sim 3$ kHz. More interesting, in the $1 \sim 2$ kHz frequency range the Stoneley velocity does not increase with frequency as fast as homogeneous permeability results do. As a result, the Stoneley velocity in this frequency range exhibits a very significant velocity decrease (around 1 kHz, this dispersion is about 20%, relative to the nonpermeable case). As frequency further increases, the velocity crosses the elastic formation velocity curves, and then approaches the velocity calculated with the inner layer permeability (the attenuation also shows the same trend), indicating the inner layer properties control the Stoneley wave propagation at high frequencies.

To further demonstrate the relative importance of the inner layer and virgin forma-

tion properties, we plot the dynamic pressure field as the function of radial distance for two extreme frequencies, 100 Hz and 5 kHz. Figure 14 shows the real and imaginary parts of the complex pressure fields for the 100 Hz (a) and 5 kHz (b) cases. For the very low frequencies, the dynamic fluid flow pressure can penetrate the inner layer to the depth of about 0.7 m into the formation. This explains why the results at very low frequencies are sensitive to the virgin formation. At high frequencies, the dynamic flow is effective only close to the borehole wall. This shows that the Stoneley wave propagation will primarily be controlled by the inner layer properties at high frequencies. The significant Stoneley wave velocity dispersion (velocity decrease or travel time delay) and attenuation peak in the frequency range of common Stoneley wave measurements can be easily measured. Therefore, the dispersion and attenuation characteristics can be used as a diagnostic of near borehole wall damage or fractures.

CONCLUSIONS

For the first time, the effects of various types of heterogeneous formation permeability on the borehole Stoneley waves have been investigated. The approach was based on an iterative finite difference technique developed for cylindrical coordinates. Because the dynamic fluid flow effects are most effective in the region around the borehole, the Stoneley wave samples the effective (or average) permeability of the immediate surrounding formation (see our modeling of random permeability formation). Because the Stoneley wave sums the effects of pore fluid flow in all azimuthal directions, the Stoneley wave is not sensitive to the permeability anisotropy (or azimuthal variation of pore fluid flow in the formation). This has been evidenced by our modeling of Stoneley wave propagation in layered porous media. In most cases, the behavior of Stoneley waves in a variable permeability formation is very similar to the behavior in a homogeneous permeability formation. This demonstrates that the analytical solution for the homogeneous permeability formation (Eq. 18) provides a very useful method for calculating the effective permeability of the heterogeneous formation surrounding the borehole, although the calculated permeability may be (slightly or moderately) higher than the average permeability of the formation depending on the degree of variation of the heterogeneity (see Figure 4).

The most likely case in which the formation permeability heterogeneities will have significant effects on the Stoneley wave propagation is the damaged zone case where the damaged borehole has much higher permeability than the virgin formation, due to fissures or micro-fractures existing at the borehole wall. As predicted by our modeling, this damaged, highly permeable wall can be detected by the significant delay in Stoneley wave arrival (up to 20% relative to the non-permeable formation) and attenuation peak in the frequency range of common Stoneley wave measurements.

APPENDIX

Iterative Finite Difference Solution of Dynamic Flow in Cylindrical Coordinates

In this appendix, we describe the finite difference solution of dynamic fluid flow in a heterogeneous permeability medium in the cylindrical coordinate system. This flow is described by Eq. (13). In the cylindrical coordinates, the flow occurs in the region

$$\begin{aligned} R_0 < \quad & r \quad < R \\ 0 < \quad & \theta \quad < 2\pi \quad , \end{aligned}$$

where R_0 is the borehole radius and R is the outer radius of the region at which the flow effectively vanishes because of the radiation condition. It is convenient to non-dimensionalize the governing equation (Eq. 13). We use the dimensionless variables r' $(0 < r' < 1)$ and θ' $(0 < \theta' < 1)$ and the transformation

$$\begin{cases} r = R_0 + (R - R_0)r' \\ \theta = 2\pi\theta' \end{cases} \tag{A.1}$$

The spatially varying dynamic fluid diffusivity $\alpha(r, \theta; \omega)$ may also be non-dimensionalized using

$$\alpha = \frac{\kappa(r, \theta; \omega) K_f}{\mu\phi} = \alpha_0 \cdot \alpha'(r, \theta; \omega) \quad , \tag{A.2}$$

where

$$\alpha_0 = \frac{\kappa_{max} K_f}{\mu\phi} \quad , \tag{A.3}$$

and

$$\alpha' = \frac{\gamma(r, \theta)}{\left[1 - \frac{i}{2}\tau\kappa_{max}\gamma(r, \theta)\frac{\rho_f\omega}{\mu}\phi\right]^{1/2} - i\tau\kappa_{max}\gamma(r, \theta)\frac{\rho_f\omega}{\mu\phi}} \quad , \tag{A.4}$$

where κ_{max} is the maximum permeability in the model, $\gamma(r, \theta) = \frac{\kappa(r, \theta)}{\kappa_{max}}$ is the dimensionless permeability distribution. $\alpha'(r, \theta; \omega)$ is now the dimensionless diffusivity that is a function of both frequency and spatial position. The non-dimensionalized governing equation becomes

$$\frac{\partial}{\partial r'}\left(\alpha'\frac{\partial p}{\partial r'}\right) + \frac{R - R_0}{R_0 + (R - R_0)r'}\alpha'\frac{\partial p}{\partial r'} + \frac{(R - R_0)^2}{4\pi^2[R_0 + (R - R_0)r']^2}\frac{\partial}{\partial\theta'}\left(\alpha'\frac{\partial p}{\partial\theta'}\right) + (i\beta - \alpha' k_e^2)p = 0 \quad , \tag{A.5}$$

where $\beta = \frac{\omega}{\alpha_0}(R - R_0)^2$ is the dimensionless frequency.

Using the following notations, Eq. (A.5) can be written as

$$A_1 p + A_2 p + A_3 p + A_4 p = 0 \tag{A.6}$$

where the operators A_i (i = 1, 2, 3, 4) are

$$\begin{cases} A_1 = \dfrac{\partial}{\partial r'}\left(\alpha' \dfrac{\partial}{\partial r'}\right) \\ A_2 = \dfrac{R - R_0}{R_0 + (R - R_0)r'} \alpha' \dfrac{\partial}{\partial r'} \\ A_3 = \dfrac{(R - R_0)^2}{4\pi^2 [R_0 + (R - R_0)r']^2} \dfrac{\partial}{\partial \theta'}\left(\alpha' \dfrac{\partial}{\partial \theta'}\right) \\ A_4 = i\beta - \alpha' k_e^2. \end{cases} \tag{A.7}$$

Because the straightforward center difference solution of Eq. (A.6) is unstable (Zhao et al., 1992), we instead solve Eq. (A.6) using an iterative finite difference technique (Zhao et al., 1992). We find the solution for the following equation

$$A_1 p + A_2 p + A_3 p + A_4 p = \frac{\partial p}{\partial t'} \ , \tag{A.8}$$

where t' is a dimensionless time. The solution of Eq. (A.8) can be computed iteratively with increasing t' to approach the steady state, at which the solution of Eq. (A.8) will be the solution of (A.6) (Zhao et al., 1992). Eq. (A.8) can be solved using the ADI (Alternating Direction Implicit) method which is unconditionally stable for Eq. (A.8) type equations (Ferziger, 1981; Zhao et al., 1992). Using the ADI finite difference method, we discretize the dimensionless variables r', θ' and t' using

$$\begin{cases} r' = i\Delta r' & i = 0, 1, 2, \cdots, I & \Delta r' = 1/I \\ \theta' = j\Delta\theta' & j = 0, 1, 2, \cdots, J & \Delta\theta' = 1/J \\ t' = n\Delta t' & n = 0, 1, 2, \cdots, N. & \end{cases} \tag{A.9}$$

For practical purposes $\Delta t'$ can be chosen to be $\Delta r'/2$. To use the ADI method, we rewrite Eq. (A.8) as

$$A_5 p + A_3 p = \frac{\partial p}{\partial t'} \tag{A.10}$$

where

$$A_5 p = A_1 p + A_2 p + A_4 p. \tag{A.11}$$

Eq. (A.10) can be solved using the Peaceman-Rachford algorithm (Ferziger, 1981). This algorithm consists of splitting Eq. (A.10) into two separate equations by using an intermediate function $p^{n+1/2}$:

$$\left(I-\frac{\Delta t'}{2}A_{5h}\right)p^{n+1/2}=\left(I+\frac{\Delta t'}{2}A_{3h}\right)p^{n} \tag{A.12}$$

$$\left(I-\frac{\Delta t'}{2}A_{3h}\right)p^{n+1}=\left(I+\frac{\Delta t'}{2}A_{5h}\right)p^{n+1/2}\ , \tag{A.13}$$

where I is unit matrix; A_{3h} and A_{5h} are finite difference operators, which, when operated on p, can be written as:

$$\begin{cases} A_{5h}p &= \frac{1}{\Delta r'^2}\left[(B_{i,j}-D_{i,j})p_{i-1,j}-\left(B_{i,j}+B_{i+1,j}-D^{(1)}_{i,j}\right.\right. \\ &\qquad \left.\left.-(\frac{i\omega}{\alpha_0}-A_{i,j}k_e^2)(R-R_0)^2\Delta r'^2\right)p_{i,j}+B_{i+1,j}p_{i+1,j}\right] \\ A_{3h}p &= D^{(2)}_{i,j}\frac{1}{\Delta\theta'^2}\left[C_{i,j}p_{i,j-1}-(C_{i,j}+C_{i,j-1})p_{i,j}+C_{i,j+1}p_{i,j+1}\right]\ , \end{cases} \tag{A.14}$$

where

$$\begin{cases} A_{i,j} &= \alpha_{i,j} \\ B_{i,j} &= \dfrac{A_{i,j}+A_{i-1,j}}{2} \\ C_{i,j} &= \dfrac{A_{i,j}+A_{i,j-1}}{2} \\ D^{(1)}_{i,j} &= \dfrac{(R-R_0)B_{i,j}\Delta r'}{[R_0+(R-R_0)(r'_{i,j}+r'_{i-1,j})/2]} \\ D^{(2)}_{i,j} &= \dfrac{(R-R_0)^2}{4\pi^2[R_0+(R-R_0)r'_{i,j}]^2}. \end{cases} \tag{A.15}$$

Therefore, the finite difference form of Eq. (A.10) is

$$\begin{aligned} &-\mu_1(B_{i,j}-D^{(1)}_{i,j})p^{n+1/2}_{i-1,j}+\left[1+\mu_1(B_{i,j}+B_{i+1,j}-D^{(1)}_{i,j}\right. \\ &\qquad \left.-(i\tfrac{\omega}{\alpha_0}-A_{i,j}k_e^2)\Delta r'^2(R-R_0)^2)\right]p^{n+1/2}_{i,j}-\mu_1 B_{i+1,j}p^{n+1/2}_{i+1,j} \\ &\quad =\mu_2 D^{(2)}_{i,j}p^{n}_{i,j-1}+\left[1-(C_{i,j}+C_{i,j+1})\mu_2 D^{(2)}_{i,j}\right]p^{n}_{i,j}+\mu_2 D^{(2)}_{i,j}C_{i,j+1}p^{n}_{i,j+1}. \end{aligned} \tag{A.16}$$

$$\begin{aligned} &-\mu_2 D^{(2)}_{i,j}C_{i,j}p^{n+1}_{i,j-1}+\left[1+\mu_2 D^{(2)}_{i,j}(C_{i,j}+C_{i,j+1})\right]p^{n+1}_{i,j}-\mu_2 D^{(2)}_{i,j}C_{i,j+1}p^{n+1}_{i,j+1} \\ &\quad =\mu_1(B_{i,j}-D^{(1)}_{i,j})p^{n+1/2}_{i-1,j}+\left[1-\mu_1\left(B_{i,j}+B_{i+1,j}-D^{(1)}_{i,j}\right.\right. \\ &\qquad \left.\left.-(i\tfrac{\omega}{\alpha_0}-A_{i,j}k_e^2)(R-R_0)^2\Delta r'^2\right)\right]p^{n+1/2}_{i,j}+\mu_1 B_{i+1,j}p^{n+1/2}_{i+1,j} \end{aligned} \tag{A.17}$$

The ADI method introduces an intermediate function $p^{n+\frac{1}{2}}$ between p^n and p^{n+1}. The advantage of the using $p^{n+\frac{1}{2}}$ can be seen from Eqs. (A.16) and (A.17). The solution procedure begins at $t' = 0$, at which the initial condition $p^{n=0}$ is given. Because we are only interested in the steady state solution, the initial condition can be arbitrarily chosen, e.g., $p^0(r', \theta') = 1$. Suppose that the procedure iterates from $t' = 0$ to $t' = n\Delta t'$ to produce the solution p^n for all $r' = i\Delta r'$ and $\theta' = j\Delta\theta'$. At this stage, all the terms on the right-hand side of Eq. (A.16) are known. Eq. (A.16) now becomes an one-dimensional (1-D) difference equation for $p^{n+\frac{1}{2}}$ in the r' direction, which can be solved to find $p^{n+\frac{1}{2}}$ with the given boundary condition at $r' = 0$ and $r' = 1$. Once $p^{n+\frac{1}{2}}$ is found, the terms on the right-hand side of Eq. (A.17) are known, and Eq. (A.17) is now another 1-D difference equation for p^{n+1} in the θ' direction, and can be solved with the given boundary condition at $\theta' = 0$ and $\theta' = 1$.

We now describe the solution procedure that incorporates the boundary conditions. The continuity boundary condition at the borehole wall and the radiation condition at R ($>> R_0$) are given by

$$p(0, j) = P_0 \qquad \text{and} \qquad p(I, j) = 0 \ . \tag{A.18}$$

Eq. (A.16) can be simplified into

$$a_i p_{i-1,j}^{n+1/2} + b_i p_{i,j}^{n+1/2} + c_i p_{i+1,j}^{n+1/2} = r_i^n \qquad i = 1, 2, \cdots, I-1 \ , \tag{A.19}$$

where r_i^n is the right-hand side terms of Eq. (A.16) and a_i, b_i, and c_i are the coefficients of $p_{i-1,j}^{n+1/2}$, $p_{i,j}^{n+1/2}$, and $p_{i+1,j}^{n+1/2}$ in the left-hand side of the equation. Eq. (A.19) is a tridiagonal system, which, together with appropriate boundary conditions of $p^{n+1/2}$, can be solved using the Thomas algorithm (Ferziger, 1981).

To get the boundary conditions for $p^{n+1/2}$, we start from Eqs. (A.12) and (A.13). From Eq. (A.12), we have

$$\frac{\Delta t'}{2} A_{5h} p^{n+1/2} = p^{n+1/2} - \left(I + \frac{\Delta t'}{2} A_{3h} \right) p^n \ . \tag{A.20}$$

Substituting Eq. (A.20) into (A.13), we get

$$p^{n+1/2} = \left(I - \frac{\Delta t'}{2} A_{3h} \right) p^{n+1} + \left(I + \frac{\Delta t'}{2} A_{3h} \right) p^n . \tag{A.21}$$

Subsituting Eq. (A.14) into (A.21) results in

$$p_{i,j}^{n+1/2} = \left\{ -\mu_2 D_{i,j}^{(2)} C_{i,j} p_{i,j-1}^{n+1} + \left[1 + \mu_2 D_{i,j}^{(2)} (C_{i,j} + C_{i,j+1}) \right] p_{i,j}^{n+1} - \mu_2 D_{i,j}^{(2)} C_{i,j+1} p_{i,j+1}^{n+1} \right.$$
$$\left. + \mu_2 D_{i,j}^{(2)} p_{i,j-1}^{n} + \left[1 - \mu_2 D_{i,j}^{(2)} (C_{i,j} + C_{i,j+1}) \right] p_{i,j}^{n} + \mu_2 D_{i,j}^{(2)} C_{i,j+1} p_{i,j+1}^{n} \right\} / 2 \quad . \tag{A.22}$$

At $i = 0$ and $i = I$, $p_{0,j}^{n}$, $p_{I,j}^{n}$, $p_{0,j}^{n+1}$, and $p_{I,j}^{n+1}$ are all given by the boundary conditions (Eq. (A.18)). Therefore $p_{0,j}^{n+1/2}$ and $p_{I,j}^{n+1/2}$ can be obtained as

$$\begin{cases} p_{0,j}^{n+1/2} = \beta_0 \\ p_{I,j}^{n+1/2} = \beta_I \end{cases} \tag{A.23}$$

where β_0 and β_I are the values of the right-hand side of Eq. (A.22) evaluated at $i = 0$ and $i = I$, respectively. Now the problem is to solve Eq. (A.19) for boundary conditions (A.23).

By using Gaussian elimination, we want to replace Eq. (A.19) by a relationship of the form

$$p_{i,j}^{n+1/2} = s_{i+1} p_{i+1,j}^{n+1/2} + q_{i+1} \qquad i = 1, 2, \cdots, I-1 \quad , \tag{A.24}$$

where s_{i+1} and q_{i+1} are to be determined.

Substituting Eq. (A.24) into (A.19) for $p_{i-1,j}^{n+1/2}$, we have

$$a_i (s_i p_{i,j}^{n+1/2} + q_i) + b_i p_{i,j}^{n+1/2} + c_i p_{i+1,j}^{n+1/2} = r_i \tag{A.25}$$

or

$$p_{i,j}^{n+1/2} = -\frac{c_i}{a_i s_i + b_i} p_{i+1,j}^{n+1/2} + \frac{r_i - a_i q_i}{a_i s_i + b_i} \quad . \tag{A.26}$$

Comparing (A.26) with (A.24), we must have

$$\begin{cases} s_{i+1} = -\dfrac{c_i}{a_i s_i + b_i} \\ q_{i+1} = \dfrac{r_i - a_i q_i}{a_i s_i + b_i} \end{cases} \tag{A.27}$$

for consistency of the formulas. Thus if we know s_1 and q_1, then we can calculate s_i and q_i for i greater than 1. The values of s_1 and q_1 are obtained from the boundary conditions (Eq. A.23). At $i = 0$, we have

$$p_{0,j}^{n+1/2} = s_1 p_{i,j}^{n+1/2} + q_1 = \beta_0 \,. \tag{A.28}$$

These conditions are consistent if $s_1 = 0$ and $q_1 = \beta_0$. Then s_i and q_i can be computed using Eq. (A.27). To get the value of $p_{i,j}^{n+1/2}$, we use (A.24) starting with $p_{I,j}^{n+1/2} = \beta_I$ Eq.(A.23).

To solve Eq. (A.17) for p^{n+1} using the obtained $p^{n+1/2}$, the boundary conditions at $\theta' = 0$ and $\theta' = 1$ are needed, which are periodic conditions in our cylindrical geometry. That is

$$p_{i,0} = p_{i,J} \,. \tag{A.29}$$

Again, Eq. (A.17) can be written as

$$a_j p_{i,j-1}^{n+1} + b_j p_{i,j}^{n+1} + c_j p_{i,j+1}^{n+1} = r_j \qquad j = 1, 2, \cdots, J \,. \tag{A.30}$$

The boundary conditions are

$$\begin{cases} p_{i,0}^{n+1} = p_{i,J}^{n+1} \\ p_{i,J+1}^{n+1} = p_{i,1}^{n+1} \,. \end{cases} \tag{A.31}$$

This periodic system can be solved by solving three systems as for the non-periodic case, each for $i = 1, 2, \cdots, J$:

$$\begin{cases} a_j x_{j-1} + b_j x_j + c_j x_{j+1} = r_j \\ x_0 = 0 \\ x_{J+1} = 0 \end{cases} \tag{A.32}$$

$$\begin{cases} a_j y_{j-1} + b_j y_j + c_j y_{j+1} = 0 \\ y_0 = 1 \\ y_{J+1} = 0 \end{cases} \tag{A.33}$$

and

$$\begin{cases} a_j z_{j-1} + b_j z_j + c_j z_{j+1} = 0 \\ z_0 = 0 \\ z_{J+1} = 1 \, . \end{cases} \tag{A.34}$$

Systems (A.32), (A.33), and (A.34) can be solved using the approach we have described earlier while solving for $p^{n+1/2}$ (Eqs. A.24 through A.28). The solution to the periodic system can be constructed as

$$p_{i,j}^{n+1} = x_j + g y_j + h z_j \, . \tag{A.35}$$

We choose g and h to guarantee the periodicity. For $p_{i,0}^{n+1} = p_{i,J}^{n+1}$, we have

$$x_0 + g y_0 + h z_0 = g = x_J + g y_J + h z_J \, . \tag{A.36}$$

For $p_{i,J+1}^{n+1} = p_{i,1}^{n+1}$, we have

$$x_{J+1} + g y_{J+1} + h z_{J+1} = h = x_1 + g y_1 + h z_1 \quad . \tag{A.37}$$

These are two equations with two unknowns g and h. The solution is

$$\begin{cases} g = \dfrac{x_J(1 - z_1) + x_1 z_J}{D} \\ h = \dfrac{x_J y_1 + x_1(1 - y_J)}{D} \end{cases} \tag{A.38}$$

where $D = (1 - y_J)(1 - z_1) - y_1 z_J$.

ACKNOWLEDGEMENTS

This research was supported by the Borehole Acoustics and Logging Consortium at M.I.T. and by Department of Energy Grant DE-FG02-86ER13636.

REFERENCES

Biot, M.A., 1956a, Theory of propagation of elastic waves in a fluid-saturated porous solid, I: Low frequency range, *J. Acoust. Soc. Am., 28*, 168–178.

Biot, M.A., 1956b, Theory of propagation of elastic waves in a fluid-saturated porous solid, II: Higher frequency range, *J. Acoust. Soc. Am., 28*, 179–191.

Chang, S.K., H.L. Liu, and D.L. Johnson, 1988, Low frequency tube waves in permeable rocks, *Geophysics, 53*, 519–527.

Cheng, C.H., J. Zhang, and D.R. Burns, Effects of in-situ permeability on the propagation of Stoneley (tube) waves in a borehole, *Geophysics, 52*, 1279–1289.

Cheng, C.H. and M.N. Toksöz, 1981, Elastic wave propagation in a fluid-filled borehole and synthetic acoustic logs, *Geophysics, 46*, 1042–1053.

Ferziger, J.H., 1981, *Numerical Methods for Engineering Applications*, John Wiley & Sons, Inc., New York.

Johnson, D.L., J. Koplik, and R. Dashen, 1987, Theory of dynamic permeability and tortuosity in fluid-saturated porous media, *J. Fluid Mech., 176*, 379–402.

Kerner, C., 1992, Anisotropy in sedimentary rocks modeled as random media, *Geophysics, 57*, 564–576.

Norris, A.N., 1989, Stoneley-wave attenuation and dispersion in permeable formations, *Geophysics, 54*, 330–341.

Rosenbaum, J.H., 1974, Synthetic microseismograms: logging in porous formations, *Geophysics, 39*, 14–32.

Stephen, R.A., F. Pardo-Casas, and C.H. Cheng, 1985, Finite difference synthetic acoustic logs, *Geophysics, 50*, 1588–1609.

Schmitt, D.P., M. Bouchon, and G. Bonnet, 1988, Full-wave synthetic acoustic logs in radially semi-infinite saturated porous media, *Geophysics, 53*, 807–823.

Tang, X.M. and C.H. Cheng, 1993, Borehole Stoneley wave propagation across heterogeneous and permeable structures, *Geophys. Prosp., 41*, 165–187.

Tang, X.M., C.H. Cheng, and F.L. Paillet, 1991a, Modeling Stoneley wave propoagation across in-situ fractures, *Trans. 36th Soc. Prof. Well Log Analysts*, Paper GG.

Tang, X.M., C.H. Cheng, and M.N. Toksöz, 1991b, Dynamic permeability and borehole Stoneley waves: A simplified Biot-Rosenbaum model, *J. Acous. Soc. Am., 90*, 1632–

1646.

Zhao, X.M., and M.N. Toksöz, 1991, Permeability anisotropy in heterogeneous porous media, *SEG Abstracts, D/P1.7*, 387-390.

Zhao, X.M. and M.N. Toksöz, 1992, Transient fluid flow in heterogeneous porous media, *SEG Abstracts, EG2.7*, 385–388.

Zhao, X.M., C.H. Cheng., X.M. Tang, and M.N. Toköz, 1992, Dynamic fluid flow in heterogeneous porous media and through a single fracture with rough surfaces, *M.I.T. Borehole Acoustic and Logging Consortium Report.*

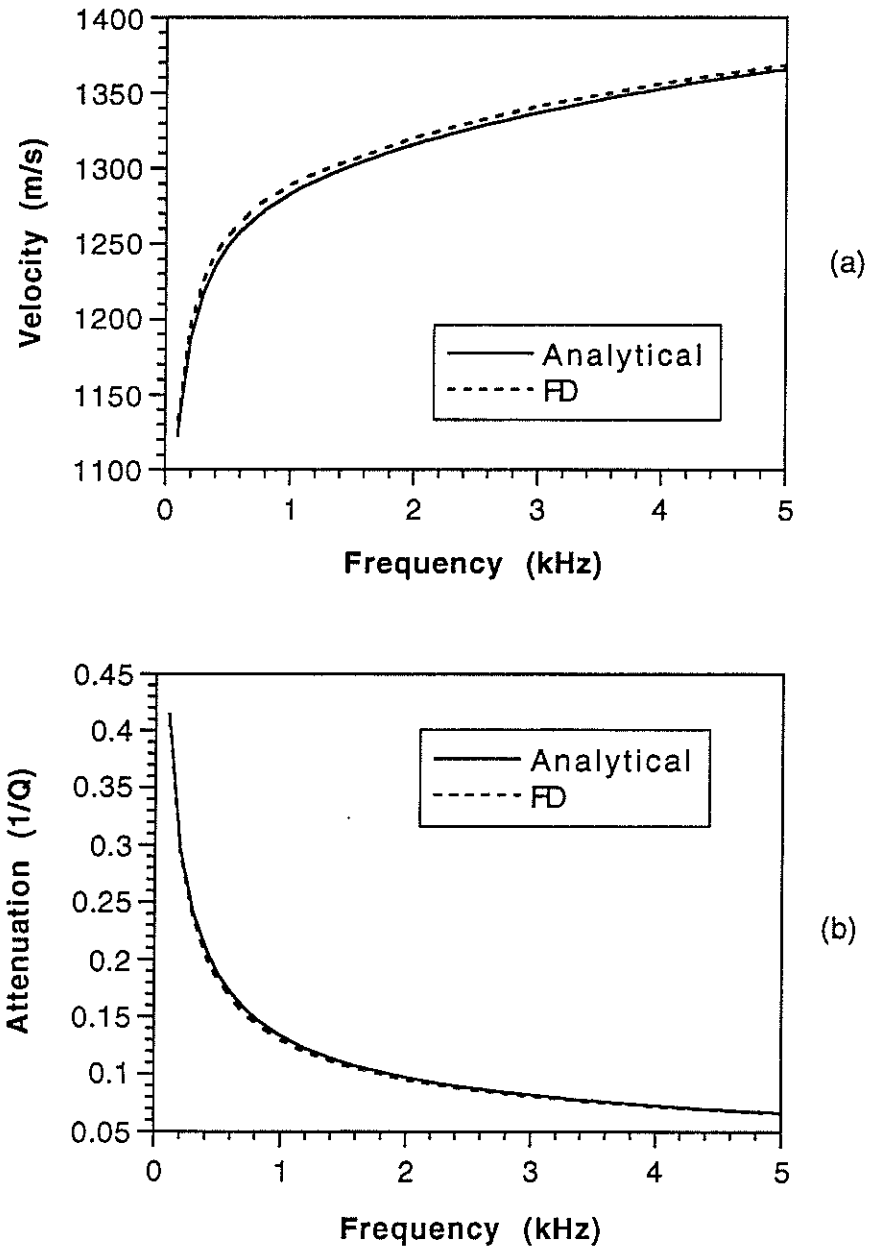

Figure 1: Comparison between analytical (dashed line) and finite difference (solid line). (a) Stoneley velocity, (b) Stoneley attenuation.

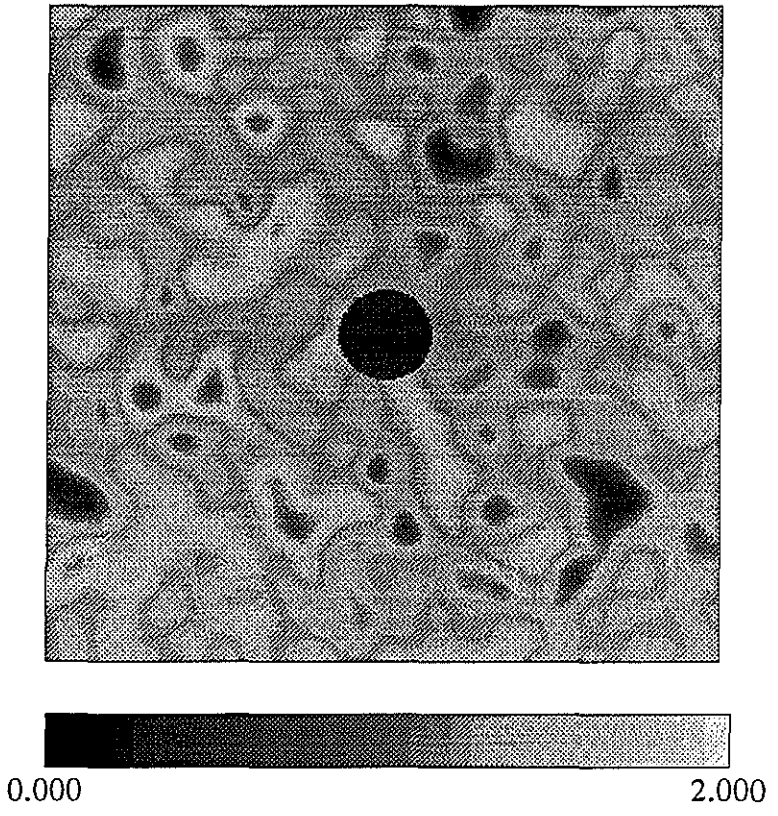

Figure 2: Random permeability variation around the borehole.

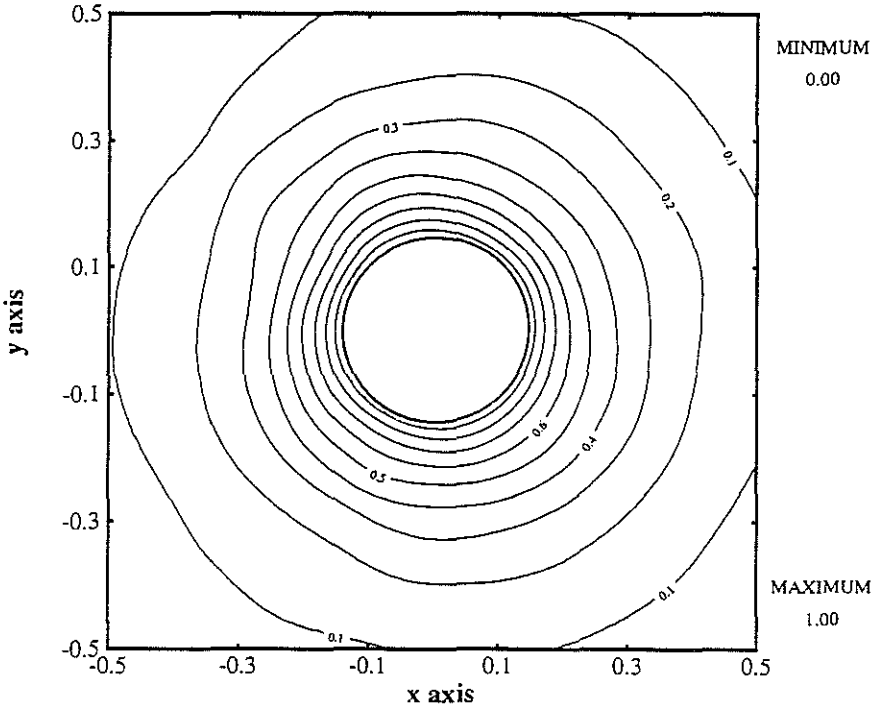

Figure 3: Contour of the amplitude of dynamic pore fluid pressure in the formation at 100 Hz.

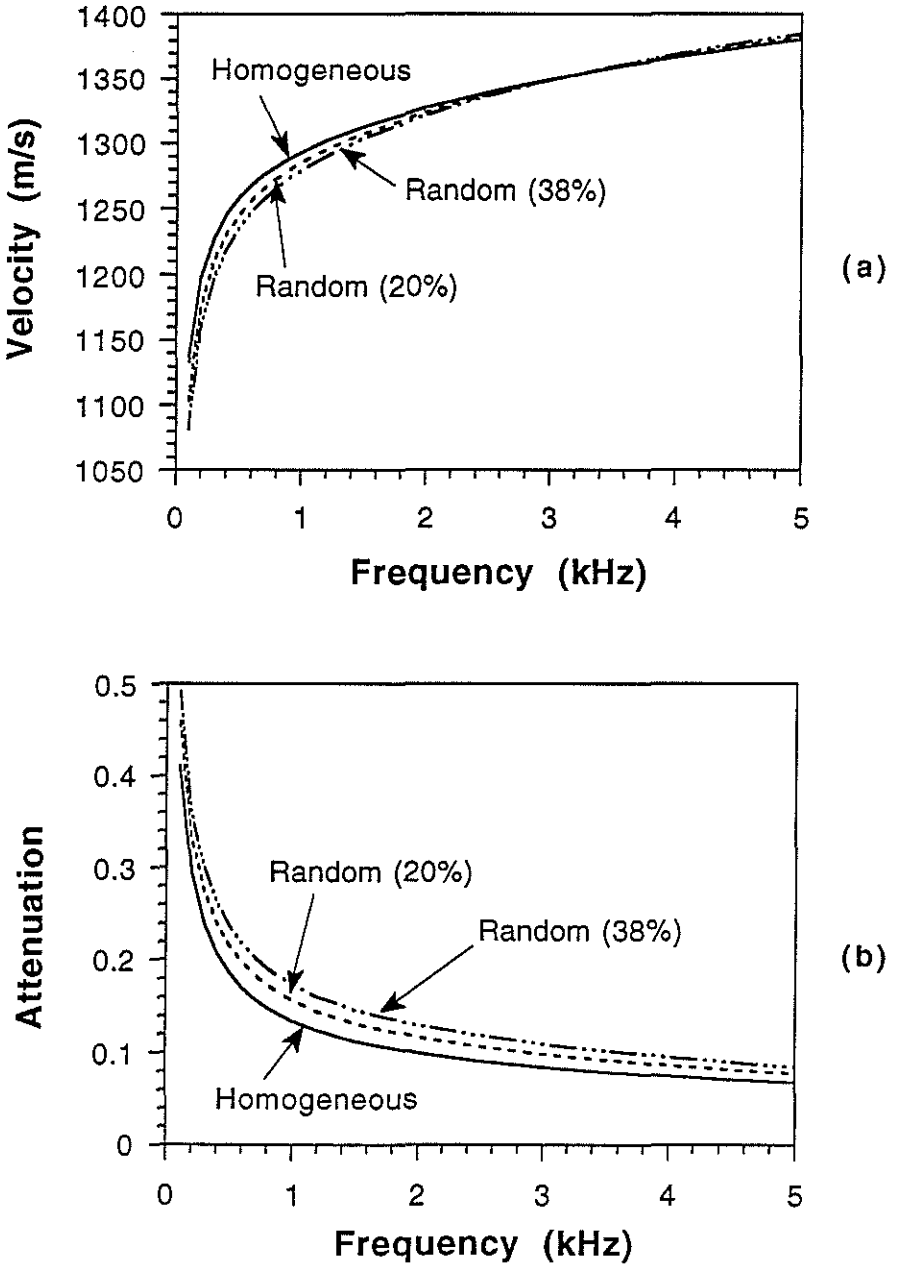

Figure 4: Stoneley wave velocity (a) and attenuation (b) due to the random permeability variation. For comparison, the results for the constant permeability are also plotted.

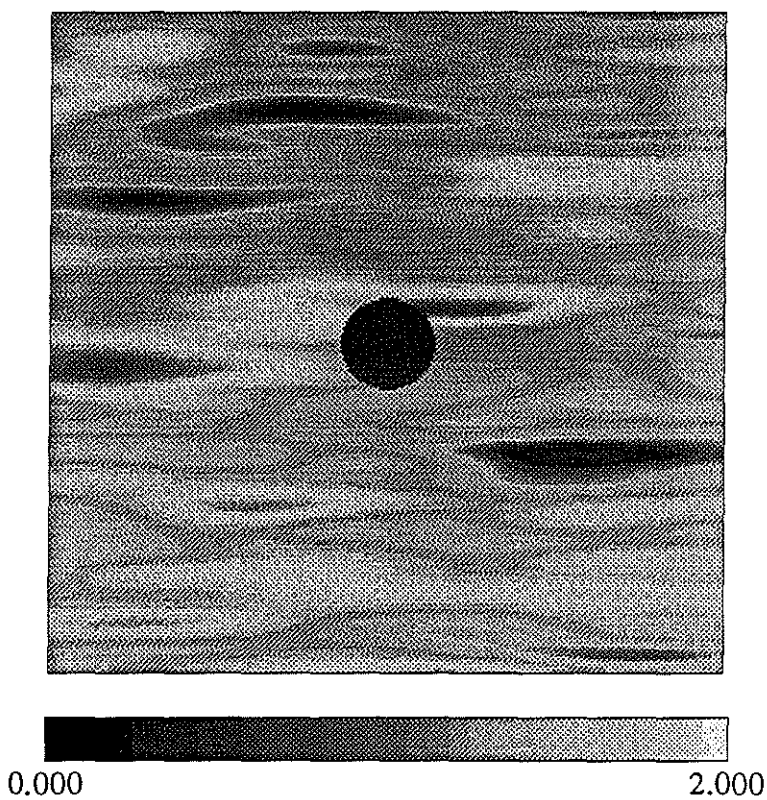

Figure 5: Lineated permeability distribution (anisotropy) surrounding the borehole (the lineation is smoothly varying).

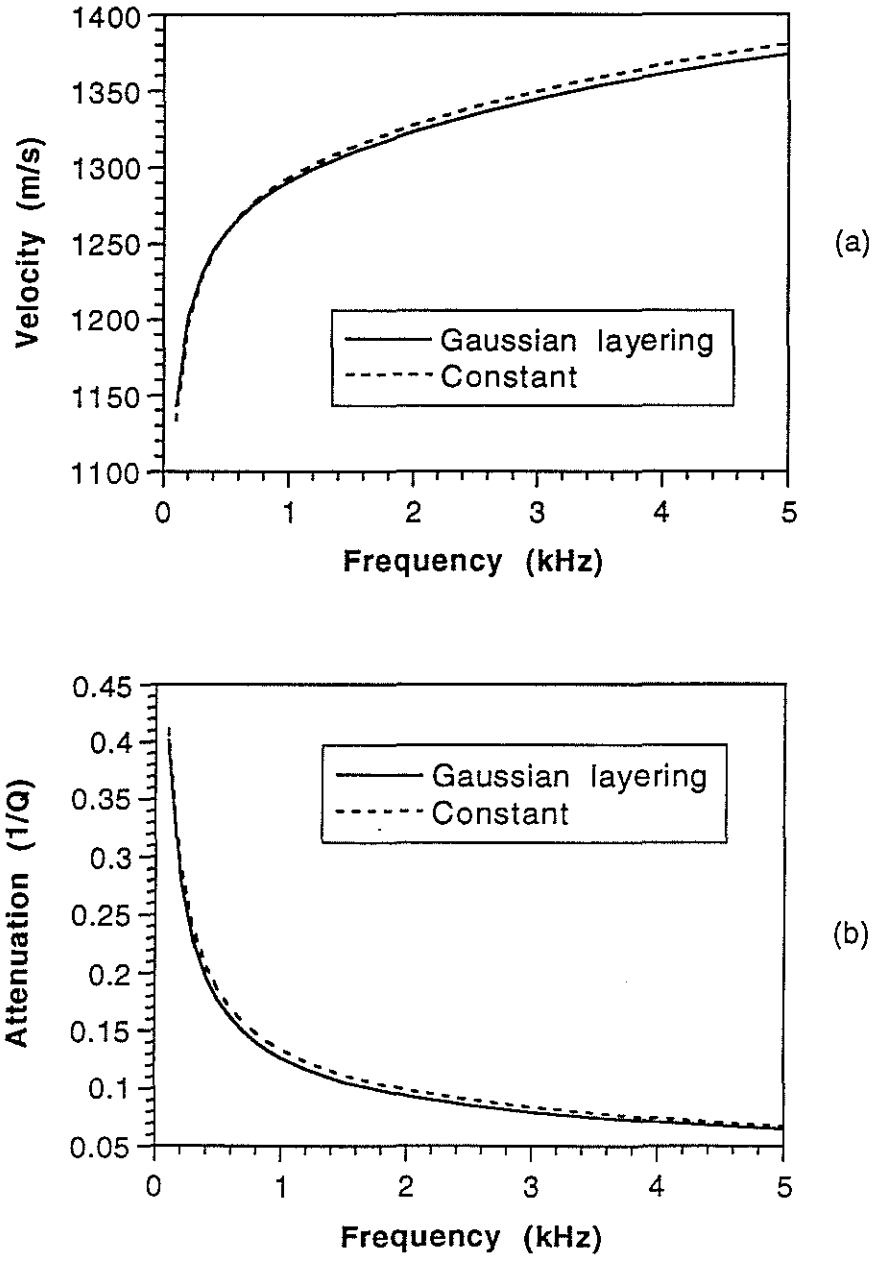

Figure 6: Stoneley wave velocity (a) and attenuation (b) due to the lineated permeability variation of Figure 6 (solid curves). The results for the constant permeability are also plotted (dashed curves).

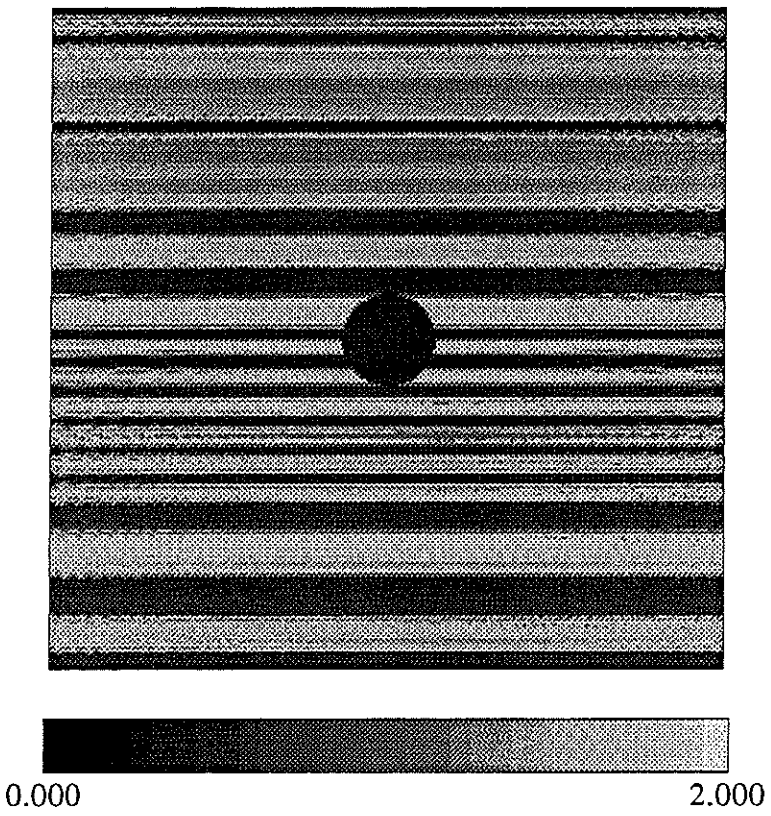

Figure 7: Laminated high- and low-permeability layers around the borehole.

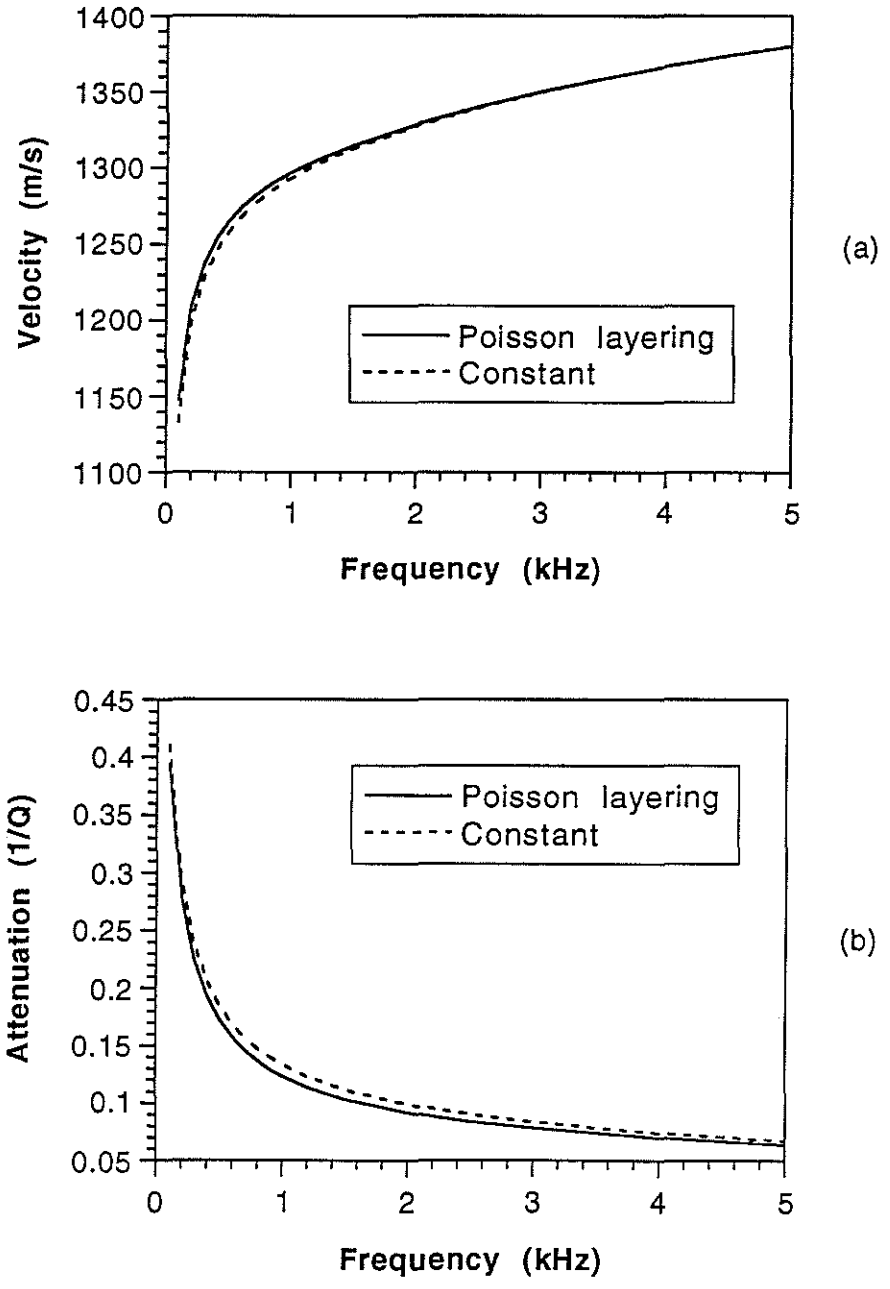

Figure 8: Stoneley wave velocity (a) and attenuation (b) due to laminated permeability variation in Figure 8. For comparison, the results for the constant permeability are also plotted.

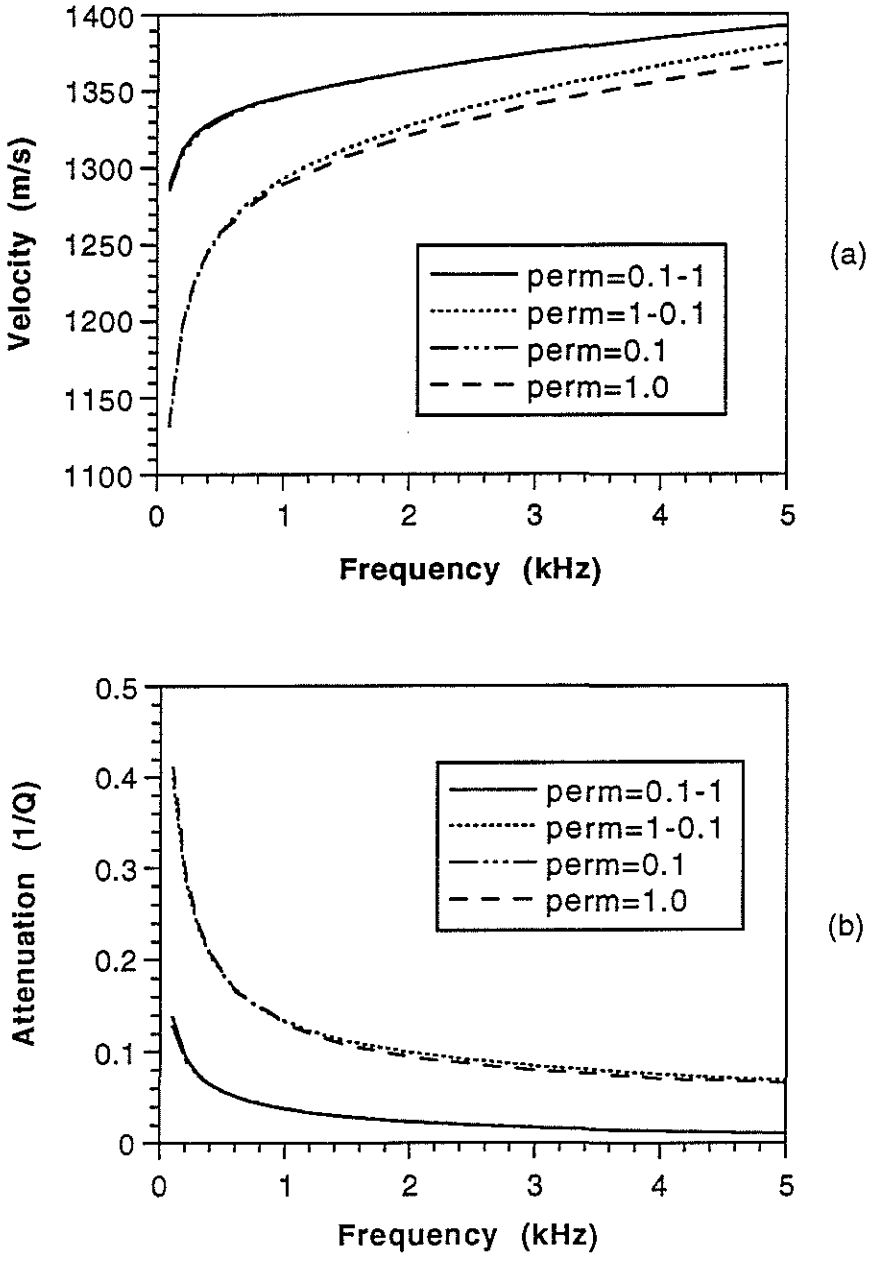

Figure 9: Stoneley wave velocity (a) and attenuation (b) for the linearly varying (increasing and decreasing) permeability models. The results of a homogeneous formation with permeability equal to 0.1 Darcy and 10 Darcy are also plotted.

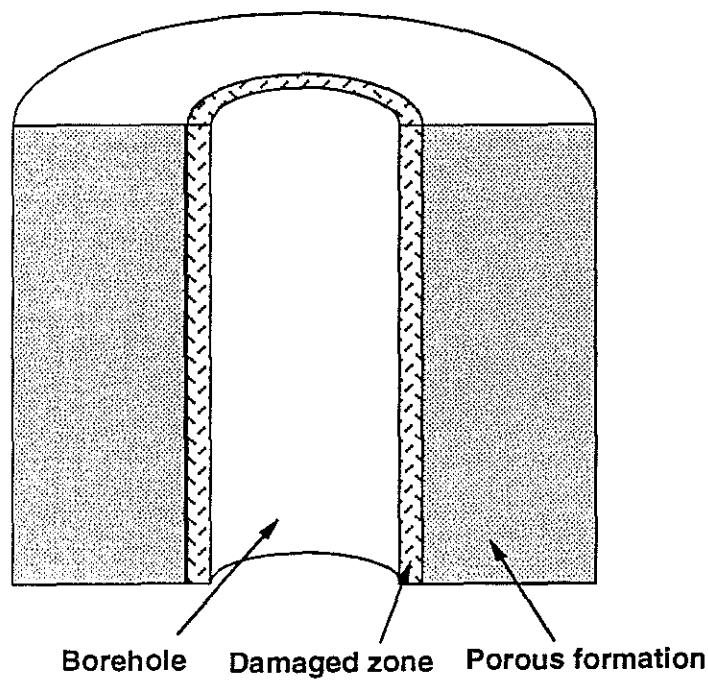

Figure 10: Modeling of a damaged borehole wall as a high permeability layer.

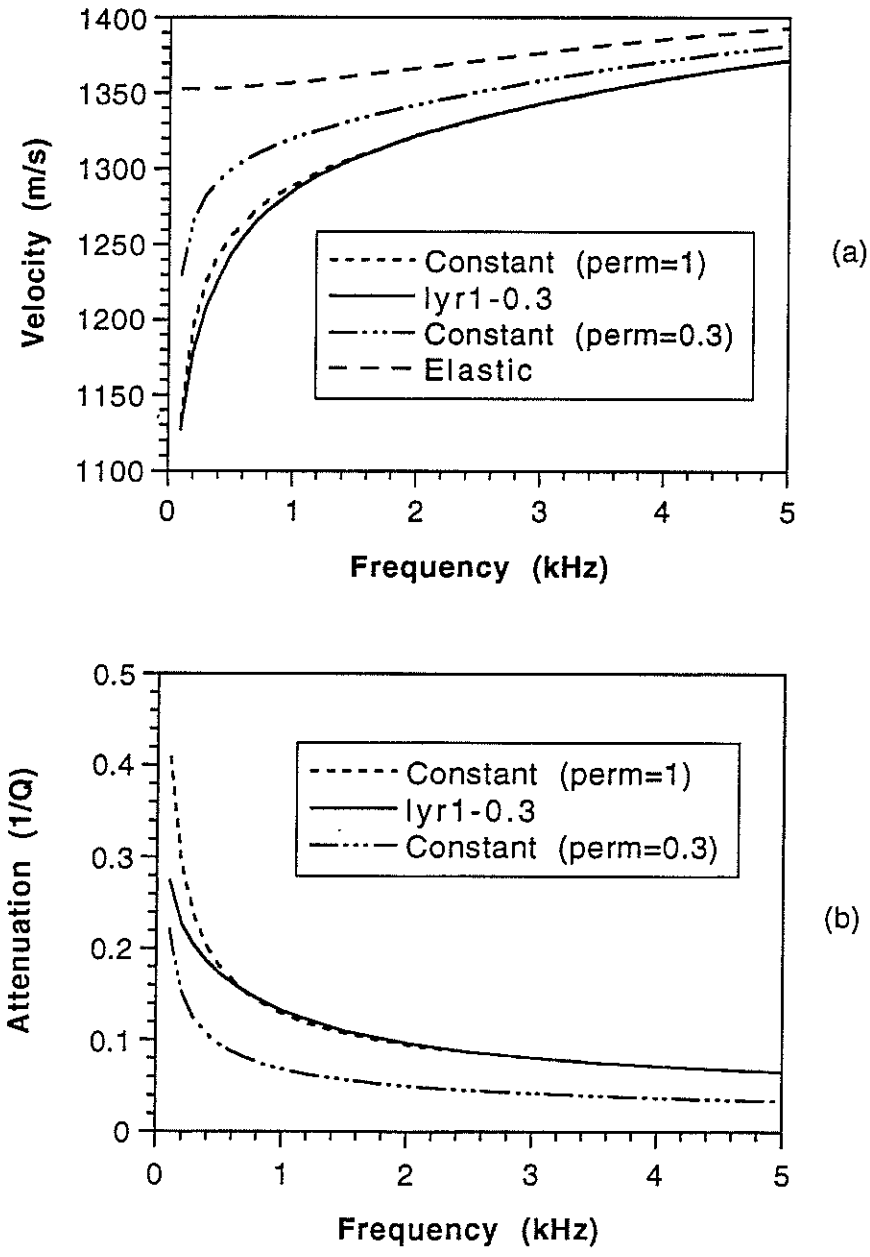

Figure 11: Stoneley wave velocity (a) and attenuation (b) for the damaged zone model. The inner layer permeability is 1 Darcy and the virgin formation is 0.3 Darcy.

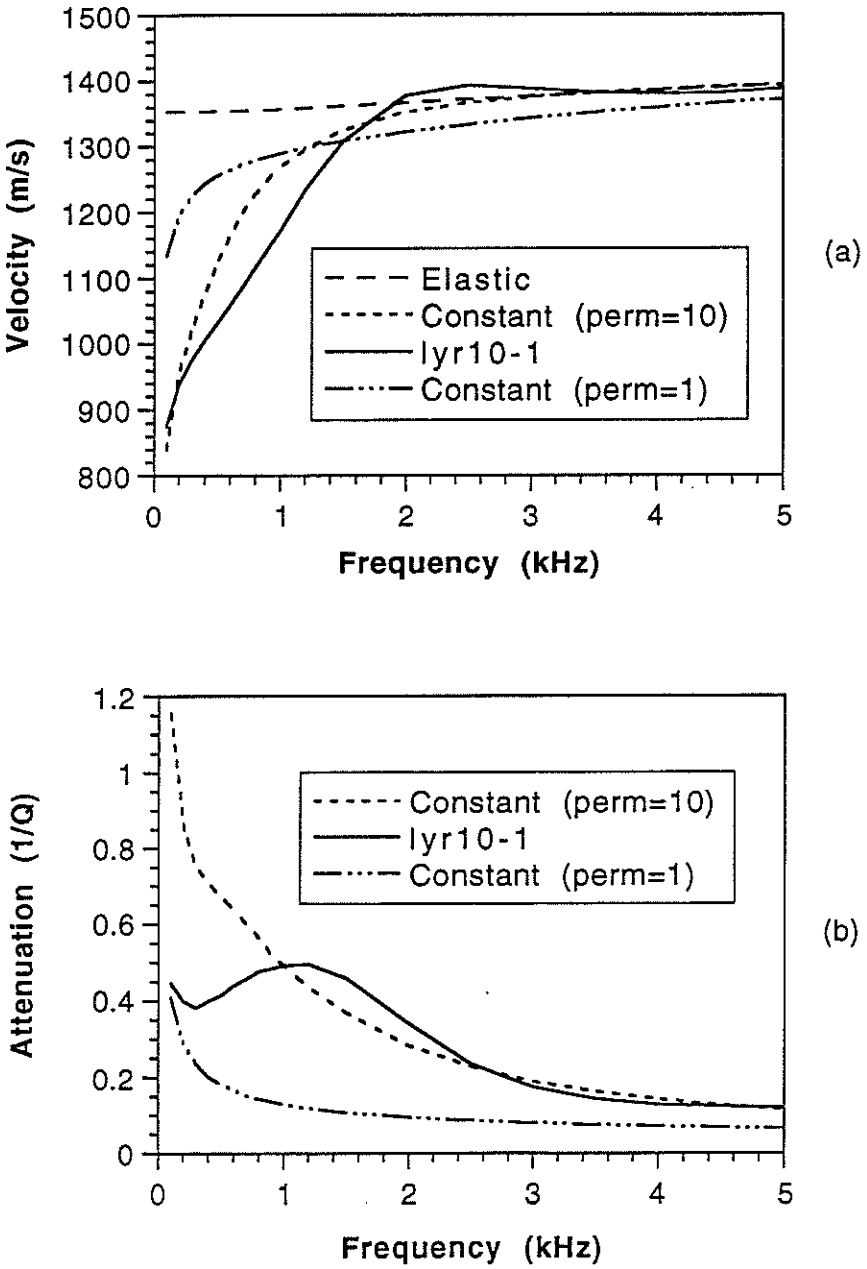

Figure 12: Stoneley wave velocity (a) and attenuation (b) for the damaged zone model. The inner layer permeability is 10 Darcy and the virgin formation permeability is 1 Darcy.

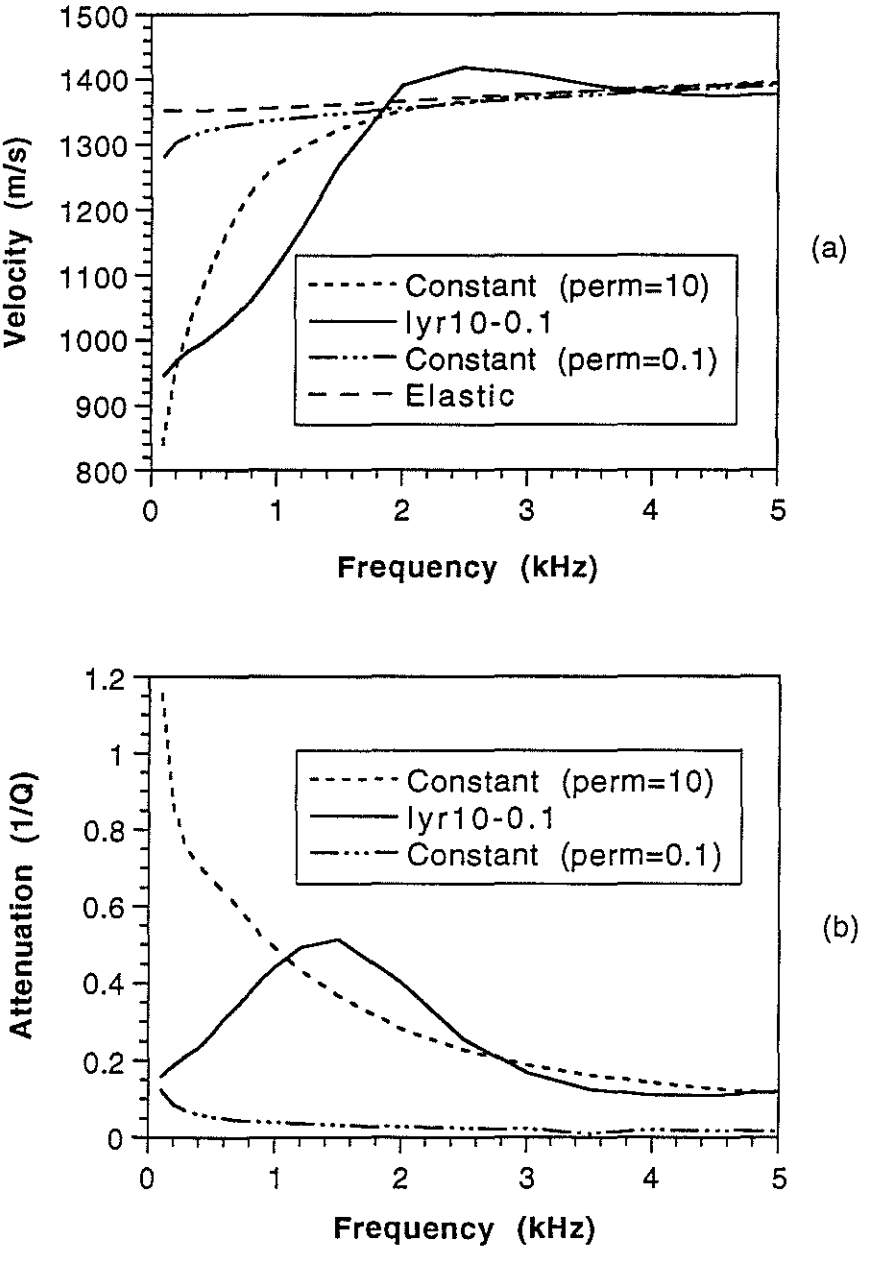

Figure 13: Stoneley wave velocity (a) and attenuation (b) for the damaged zone model. The zone permeability is 10 Darcy and the virgin formation permeability is 0.1 Darcy.

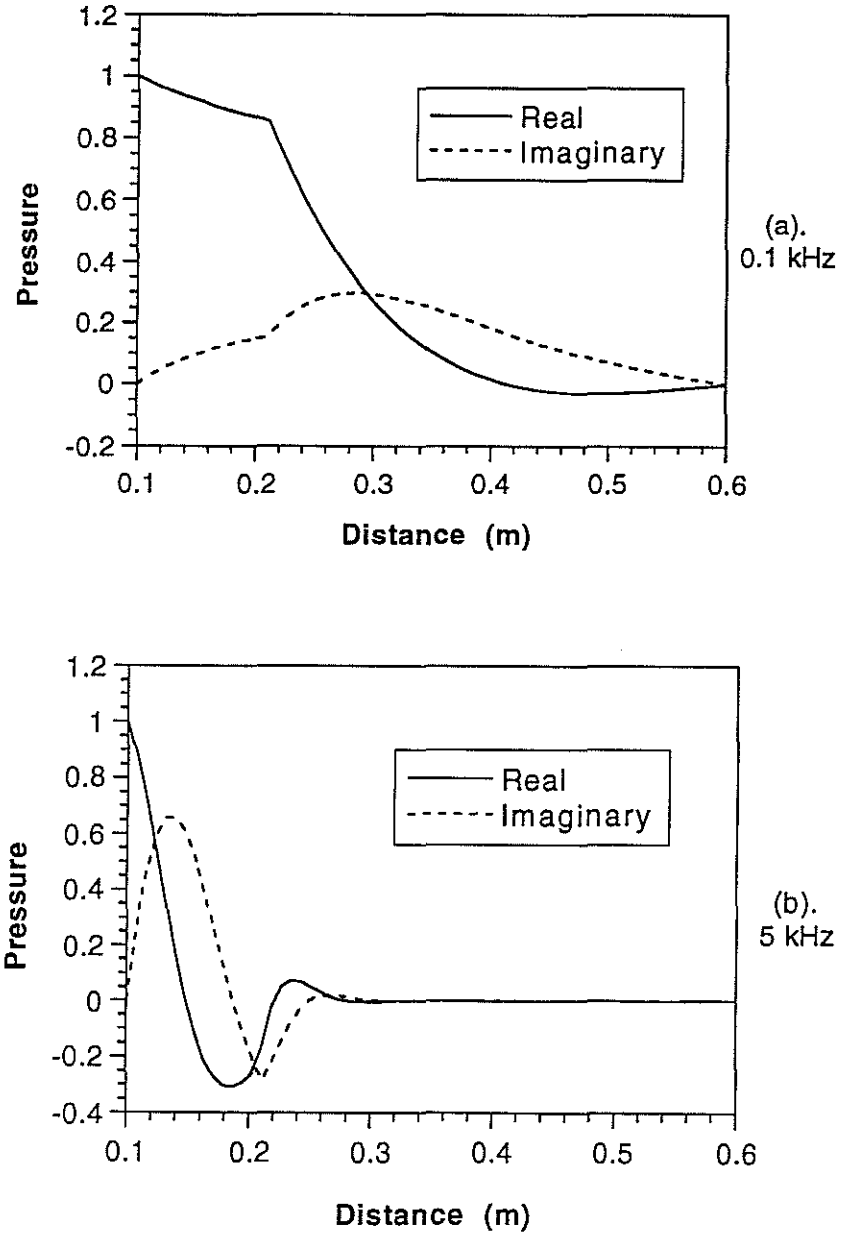

Figure 14: Amplitude of formation dynamic pore fluid pressure for the damaged zone borehole model as a function of radial distance. (a) frequency = 100 Hz. (b) frequency = 5 kHz.